Redox-Regulated Conformational Changes in an SH3 Domain[†,‡]

Jürgen Zimmermann,[§] Ronald Kühne,[||] Marc Sylvester,[§] and Christian Freund*[,§]

Protein Engineering and Molecular Modeling Group, Leibniz-Institut für Molekulare Pharmakologie und Freie Universität Berlin, 13125 Berlin, Germany

Received March 5, 2007; Revised Manuscript Received March 27, 2007

ABSTRACT: Oxidation-induced conformational changes in proteins provide a powerful mechanism to sense the redox state of a living cell. In contrast to the unspecific and often irreversible oxidation of intracellular proteins during severe oxidative stress, regulatory redox events need to have specific and transient effects on cellular targets. Here we present evidence for the reversible formation of a vicinal disulfide bond in a prototypic protein interaction domain. NMR spectroscopy was used to determine the structure of the N-terminal hSH3 domain ($hSH3^N$) of the immune cell protein ADAP (adhesion and degranulation promoting adapter protein) in the reduced and oxidized states. An eight-membered ring formed upon oxidation of two neighboring cysteines leads to significant changes in the variable arginine−threonine (RT) loop of the $hSH3^N$ domain and alters the helix−sheet packing of the domain. The redox potential for this structural transition is −228 mV at pH 7.4. This is compatible with a role of the cysteinylcysteine moiety in redox signaling during T cell activation.

The reversible oxidation of proteins offers aerobic organisms means to enhance the stability and modulate the function of proteins (*1*, *2*). In eukaryotic cells, oxidative modification of proteins, most prominently the formation of disulfide bridges between cysteines, is thought to occur primarily in the endoplasmic reticulum (*3*). According to this paradigm, the reducing environment of the cytoplasm is maintained by the reductive power of molecular guards such as glutathione or thioredoxin. However, dynamic changes in the level of reactive oxygen species (ROS)[1] have more recently been shown to modulate certain signaling cascades. Activation of several surface receptors by mitotic stimuli was shown to lead to increased levels of ROS and enhanced signaling (*1*). ROS thereby seem to complement receptor triggering and to facilitate the transactivation of surface molecules, as, for example, angiotensin II type 1 and EGF/PDGF receptors (*4*, *5*). The source of ROS apart from mitochondrial leakage is still under debate. While, in certain systems, Rac-dependent assembly and activation of nonphagocytic NADPH oxidases are likely sources of ROS (*6*, *7*), recent studies provide evidence that antibodies, the T cell receptor, or EGFR produce hydrogen peroxide extracellularly (*8*−*10*). Since H_2O_2 can pass membranes, it may affect intracellular signaling in the vicinity of receptor engagement. ROS in the cytoplasm subsequently affect signaling cascades, as, for example, MAP kinase pathways (*11*−*14*). Tyrosine phosphorylation has emerged as a pivotal step in mediating such ROS-dependent intracellular signaling events. Critically, ROS oxidize the active site cysteine of tyrosine phosphatases, thereby inhibiting enzymatic activity (*15*). As a consequence, phosphorylation by src kinases is enhanced, but it is still under debate whether ROS also induce a direct activation of the kinases (*13*). This example shows that advancement in the molecular description of redox signaling requires knowledge about oxidative modifications of proteins that make them amenable to act as biochemical sensors or signal transducers in eukaryotic cells (*16*).

In T cells, superoxide anions and hydrogen peroxide are rapidly produced after stimulation of the T cell receptor (*17*). In addition to extracellular ROS and the mitochondrial production of these species, a phagocyte-type NADPH oxidase was recently shown to contribute to FasL-Fas-dependent ROS production in T cells (*18*). This local production of ROS at the plasma membrane has the potential to modify redox-sensitive cysteines in neighboring cytoplasmic protein complexes. The phosphatase SHP-2 was shown to be inhibited by ROS, and as a consequence the signaling proteins Vav1 and ADAP downstream of SHP-2 remain hyperphosphorylated after T cell stimulation (*19*).

The T cell protein ADAP comprises a number of putative and proven protein−protein interaction motifs. In addition, ADAP contains two helically extended SH3 domains named $hSH3^N$ and $hSH3^C$, respectively These domains were identified as interesting variants of the SH3 fold that have lost the ability to bind to proline-rich sequences but show moderate affinities toward acidic phospholipids (*20*−*22*). Our investigations now show that two neighboring cysteine residues in the ADAP $hSH3^N$ domain can be reversibly oxidized and reduced in vitro, leading to pronounced changes in the HSQC spectrum of the domain. Structural analysis reveals two distinct RT loop conformations for the reduced

[†] The work was supported by a grant from the BMBF (0311879).

[‡] NMR assignments for the two forms of the domain have been deposited in the BioMagResBank under accession codes 6536 (reduced) and 6539 (oxidized). Coordinates have been deposited in the Protein Data Bank with accession codes 2GTJ (reduced) and 2GTO (oxidized).

* Corresponding author. Tel: ++49-30-94793-181. Fax: ++49-30-94793-189. E-mail: freund@fmp-berlin.de.

[§] Protein Engineering Group.

[||] Molecular Modeling Group.

[1] Abbreviations: ADAP, adhesion and degranulation promoting adaptor protein; ROS, reactive oxygen species; LUV, large unilamellar vesicles; POPC, palmitoyloleoylphosphatidylcholine; $PI(4,5)P_2$, phosphatidylinositol 4,5-bisphosphate; MLV, multilamellar vesicles; PIP_2, short for $PI(4,5)P_2$; PC, phosphatidylcholine; PS, phosphatidylserine.

10.1021/bi700437r CCC: $37.00
Published on Web 05/19/2007

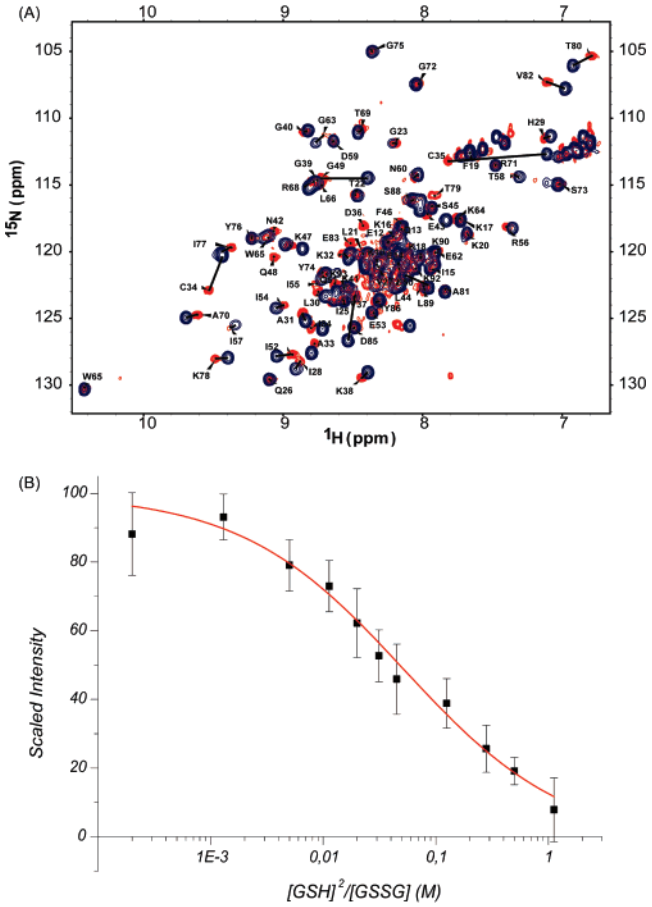

FIGURE 1: Redox properties of the hSH3^N domain of ADAP. (A) Overlay of the ^{15}N-HSQC spectra of the reduced and oxidized hSH3^N domain (reduced, red; oxidized, blue). Amino acids are labeled according to amino acid type and sequence number. Major chemical shift changes are indicated by black bars. (B) Determination of the redox potential by titration of the domain with GSH/GSSG. Plotted are the normalized and averaged peak intensities of Cys34, Cys35, Gln48, Gly49, and Thr80.

and oxidized forms of the protein and shows that a prototypic protein interaction domain can be reversibly switched at a redox potential of −228 mV. Since ADAP regulates integrin adhesion in T cells and other immune cells (*23*−*25*), this finding might be of significance for the regulation of the inside-out signaling complex.

EXPERIMENTAL PROCEDURES

Protein Expression. The nucleotide sequence corresponding to the hSH3^N domain (amino acids 490−579 of full-length ADAP; SwissProt O15117) was cloned into the pET24d vector (Novagen), and recombinant protein was expressed in *Escherichia coli* BL21(DE3) in 1xA growth medium. Protein expression was induced with 1 mM IPTG at $A_{600} = 0.5$, and cells were harvested 3 h after induction. Purification of the His-tagged hSH3^N domain from the soluble fraction of the cell lysate was achieved by Ni-NTA Sepharose chromatography. For NMR spectroscopy, 0.5−1.0 mM samples of the protein were dialyzed against 20 mM sodium phosphate and 150 mM NaCl, pH 7.4. For investigation of the oxidized or reduced form of the protein, 2 mM H_2O_2 or 2 mM dithiothreitol (DTT) was added to the sample prior to the NMR measurements, respectively.

NMR Spectroscopy. Spectra were recorded on a Bruker DRX 600 spectrometer equipped with a standard triple resonance probe and a Bruker Avance 600 spectrometer equipped with a cryoprobe. For resonance assignment and structure determination, ^{15}N-HSQC, CBCACONNH, CBCANNH, HNCO, ^{15}N-NOESY-HSQC, ^{13}C-HMQC-NOESY, and HCCH-TOCSY spectra were recorded. Generally, 16 transients with 1K complex data points were acquired for each increment, with relaxation delays between individual scans of 1−1.5 s. The mixing time for the NOESY experiments was set to 80 ms. All spectra were processed with Topspin (Bruker, Rheinstetten, Germany) and analyzed with AZARA (Wayne Boucher, unpublished) and Ansig3.3 (*26*, *27*).

Spectral Assignments and Structure Calculation. NOE spectra were manually assigned. Assignments were completed by use of CYANA2.0 (*28*−*30*) and have been deposited at the BioMagResBank [accession numbers 6536 (reduced) and 6539 (oxidized) (*31*)]. Dihedral angle restraints were derived from chemical shifts using the program TALOS (*32*). Distance and angle restraints were used as input for structure calculations with X-PLOR[5] on a Linux-based cluster. Structure calculation runs consisted of a hot phase at 1000 K for 32000 steps (64 ps), followed by 18 cooling cycles each for 5333 steps (10.66 ps) reducing the temperature by 50 K/cycle from 1000 to 100 K and followed by a final minimization phase of 1000 steps. All nonviolated structures were recalculated using a water-refinement protocol developed recently (*33*). The 20 structures closest to the average of all accepted refined structures were used for further analysis by MOLMOL (*34*) and PROCHECK-NMR (*35*). The structures were deposited in the PDB under accession codes 2GTJ (reduced) and 2GTO (oxidized).

NMR Relaxation Experiments. NMR relaxation measurements were performed at 600 MHz proton frequency, using an incrementation scheme and pulse sequence described in the literature (*36*). Curve fitting was achieved by use of the corresponding single exponential fit option in the SPARKY software package (www.cgl.ucsf.edu/home/sparky). The overall correlation times were derived from the mean values of T_1 and T_2 according to the formula (*36*):

$$\tau_C = \frac{\{[6(T_1/T_2) - 7](1/4)\}^{1/2}}{\Omega_N 2\pi}$$

where Ω_N is the larmor frequency of nitrogen (60.827865 MHz).

NMR Titration Experiment. For the redox titration, a 0.1 mM sample of the hSH3^N domain in NMR buffer (500 μL) was equilibrated against 0.2 mM reduced glutathione (GSH) and 0.2 mM oxidized glutathione (GSSG). At the beginning of the titration, the sample was in the oxidized form. The concentration of GSH was increased stepwise to 0.5, 1.0, 1.5, 2.0, 2.5, 3.0, 5.0, 7.5, 10.0, and 15.0 mM. A ^{15}N-HSQC spectrum was recorded after each addition of GSH.

Determination of the Redox Potential. For the determination of the redox potential, the intensities of several isolated peaks (Cys34, Cys35, Gln48, Gly49, Thr80) were determined in each spectrum. The highest intensity was arbitrarily scaled to 100. The intensities were plotted versus [GSH]^2/[GSSG] on a logarithmic scale and fitted against a sigmoidal decay equation. The half-point ratio of [GSH]^2/[GSSG] was

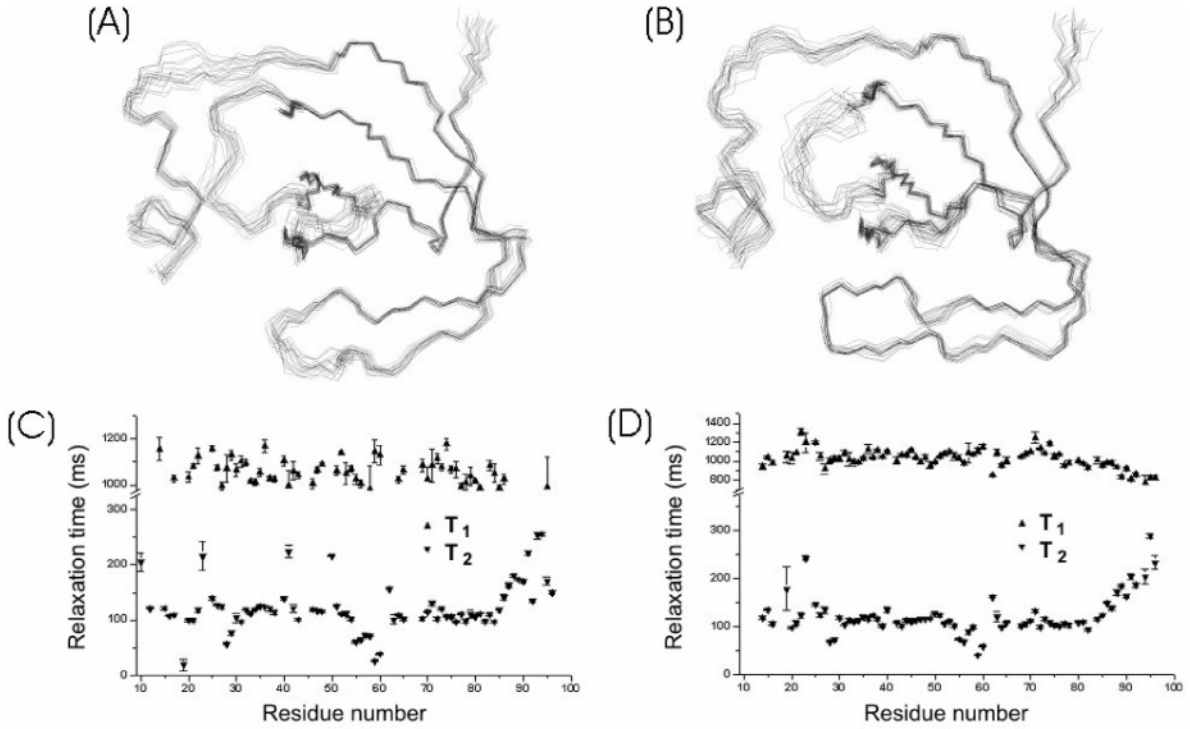

FIGURE 2: NMR investigations of reduced and oxidized hSH3^N. Backbone representations of the ensembles of the 20 lowest energy structures of the reduced (A) and oxidized (B) forms of the ADAP hSH3^N domain. In (C) and (D), T_1 and T_2 relaxation times for reduced (C) and oxidized (D) ADAP hSH3^N were fitted to an exponential decay function, and values are plotted against the amino acid sequence.

determined as 0.06 mM. Using a redox potential for the GSH/GSSG pair of −264 mV (*37*), the Nernst equation yields a redox potential of -228 ± 5 mV for the conversion between the reduced and oxidized state of the hSH3^N domain.

Large Unilamellar Vesicle (LUV) Binding Assay. LUVs were prepared by drying chloroform dissolved POPC, POPS, and PI(4,5)P_2 (Avanti Polar Lipids Inc.) in a rotary evaporator. Dried lipid films were suspended in sucrose buffer (176 mM sucrose, 10 mM MOPS, pH 7.2) and the resulting MLVs taken through five cycles of freezing (liquid nitrogen) and thawing (room temperature water bath). This was followed by 15 extrusion cycles through a polycarbonate filter of 100 nm pore size using a mini-extruder (Avanti Polar Lipids Inc.). Thereby, vesicles of a size of ∼110 nm are typically obtained, as determined by dynamic light scattering. The extruded LUVs were diluted 1:8 in liposome buffer (100 mM NaCl, 10 mM MOPS, pH 7.2) and then sedimented by centrifugation at 125000g_{max} for 1 h in a Beckman TLA-45 rotor at 25 °C. Binding assays were performed with 1.5 μM protein and 3 mM DTT (reducing conditions) or 1 mM H_2O_2 (oxidizing conditions) added to serial dilutions of LUVs in a total volume of 500 μL and incubated at room temperature for 30 min. The supernatant was immediately removed and analyzed by measurement of protein concentration using tryptophan fluorescence. For the determination of the bound fraction of hSH3^N, the following equation was derived from the law of mass action:

$$\text{fraction bound} = 1 - \{a[[(-K_D + [\text{protein}] - [\text{lipid}]_{acc}) + \sqrt{(-K_D + [\text{protein}] - [\text{lipid}]_{acc})^2 - 4(-K_D[\text{protein}])}]/2] - b\}/[\text{protein}]$$

The constants a and b account for unspecific binding events and were determined as $a = 1.02 \pm 0.03$, $b = 0.03 \pm 0.05$ for the reduced and $a = 1.04 \pm 0.04$, $b = 0.11 \pm 0.07$ for the oxidized form. The concentration of accessible lipid ([lipid]$_{acc}$) equals half the total lipid concentration.

RESULTS

Reversible Oxidation of the ADAP hSH3^N Domain. Purification of the N-terminal hSH3 domain of ADAP from *E. coli* lysates in the absence or presence of 1 mM reducing agent resulted in distinct $^{15}N-^1H$ NMR correlation spectra (Figure 1A). Large chemical shift differences were observed for Cys34/Cys35 and residues nearby, suggesting that oxidation of the cysteines is responsible for the differences in the chemical environment of NH groups in the protein. Chemical shift values of the Cβ atoms of the two cysteines are in agreement with the formation of a disulfide bond (*31*). It can be seen from Figure 1A that the chemical shift changes are not restricted to the vicinity of the two cysteines. Significant differences can be observed for residues spread over the entire domain, indicating global structural perturbations. The redox potential for the formation of the disulfide bond in the hSH3^N domain was determined by NMR spectroscopy. ^{15}N-HSQC spectra were recorded after incubating the protein with varying ratios of reduced to oxidized glutathione. A plot of averaged peak intensities against the [GSH]^2/[GSSG] ratio is shown in Figure 1B. Using the Nernst equation, the redox potential was calculated to be -228 ± 5 mV (Figure 1B).

Three-Dimensional Structure of Reduced and Oxidized hSH3^N. The three-dimensional structures of the reduced and oxidized forms of hSH3^N were determined by NMR spectroscopy. Ensembles of the 20 lowest energy structures for each form are shown in Figure 2A, and details of the structural statistics are listed in Table 1. Both forms of the protein show the anticipated SH3 domain fold flanked by a

Table 1: Statistics of Structure Calculations

	hSH3^N, reduced	hSH3^N, oxidized
no. of NOE distance constraints		
total NOE	1072	852
long range ($\|i - j\| > 3$)	583	459
total dihedral angle restraints		
ϕ	40	54
ψ	37	55
structure statistics		
violations (mean and SD)		
distance constraints (Å)	$(0.024 \pm 3) \times 10^{-4}$	$(0.026 \pm 3) \times 10^{-4}$
dihedral angle constraints (deg)	0.701 ± 0.027	0.737 ± 0.018
max dihedral angle violation (deg)	5.048	4.728
max distance constraint violation (Å)	0.329	0.394
deviations from idealized geometry		
bond lengths (Å)	$(0.014 \pm 9) \times 10^{-5}$	$(0.013 \pm 9) \times 10^{-5}$
bond angles (deg)	1.42 ± 0.008	1.31 ± 0.009
impropers (deg)	1.65 ± 0.020	1.73 ± 0.022
average pairwise rmsd for residues 14−86 (Å)		
heavy	0.96	1.10
backbone	0.44	0.52
Ramachandran plot		
most favored region	69.9	78.6
additionally allowed region	25.7	18.3
generously allowed region	2.6	1.2
disallowed region	1.8	1.2

short N-terminal α-helix. NMR relaxation times indicate that both states are well ordered with slightly enhanced mobility for amino acids linking the helix and the sheet and for the nSrc loop of the domain (Figure 2B). From the ratio of T_1 to T_2, overall correlation times of 8.5 ns (reduced form) and 8.4 ns (oxidized form) were calculated. These values are in agreement with monomers as the predominant species in both forms, providing evidence that the oxidation is an intramolecular process. The superposition of a representative structure of each ensemble is shown in Figure 3, highlighting the structural elements that differ significantly between the two forms. The inset shows the conformation of the solvent-exposed eight-membered ring formed upon oxidation of the cysteinylcysteine moiety. The NOE network encompassing Cys34 and Cys35 was compatible with a slightly distorted *trans* but not a *cis* peptide bond conformation between the two cysteines in the oxidized hSH3^N. The formation of this ring between Cys34 and Cys35 translates into backbone atom

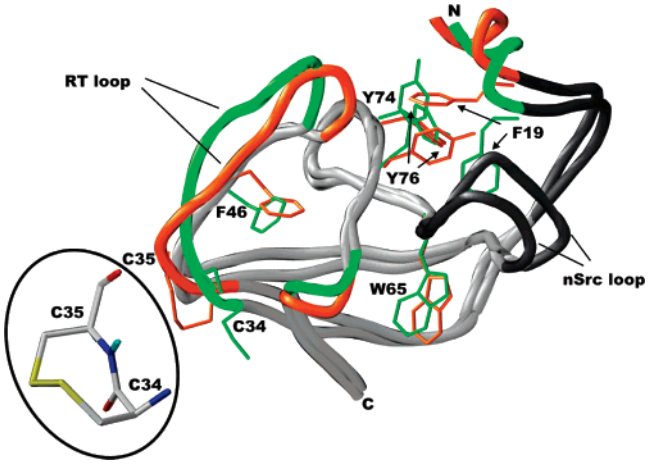

FIGURE 3: Structural changes in hSH3^N upon disulfide bond formation. The superimposed structures of the two forms of the hSH3^N domain are shown as backbone cartoons. Regions of the protein with significant changes are color coded (oxidized, orange; reduced, green) and comprise residues 13−19, 34−43, and 79−81. The backbone rmsd for these regions is 2.39 Å on average. Structurally conserved regions between the two forms are depicted in light gray; regions not well defined in the NMR ensembles (residues 20−25 and 58−64) are shown in dark gray. The side chains of the well-defined aromatic residues and cysteines are shown; hydrogen atoms are omitted for clarity. The inset shows the conformation of the eight-membered ring of the oxidized form.

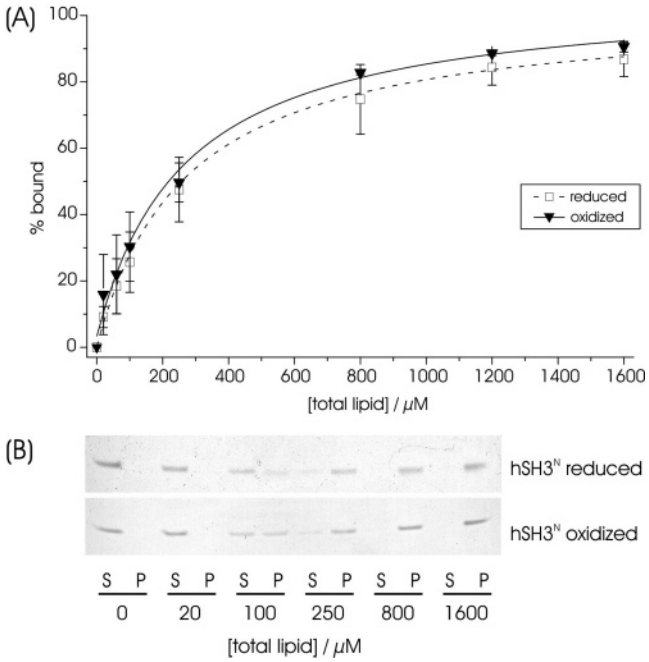

FIGURE 4: Binding of reduced and oxidized hSH3^N to PIP_2-containing liposomes. LUVs were prepared as described in Experimental Procedures. The concentrations were as follows: PC:PS:PI(4,5)P_2 = 54:44:2, [DTT], 3 mM, or [H_2O_2], 1 mM, and [hSH3^N] = 1.5 μM. (A) The average bound fraction ± SD from three independent experiments was plotted against total lipid concentration. K_D values 134 ± 17 μM (reduced) and 132 ± 23 μM (oxidized) were obtained according to the fitting procedure described in Experimental Procedures. (B) Visualization of lipid-bound and unbound protein fractions. Equal volumes of supernatant and volume-corrected pellet fractions were loaded on a SDS−PA gel and stained with Coomassie blue.

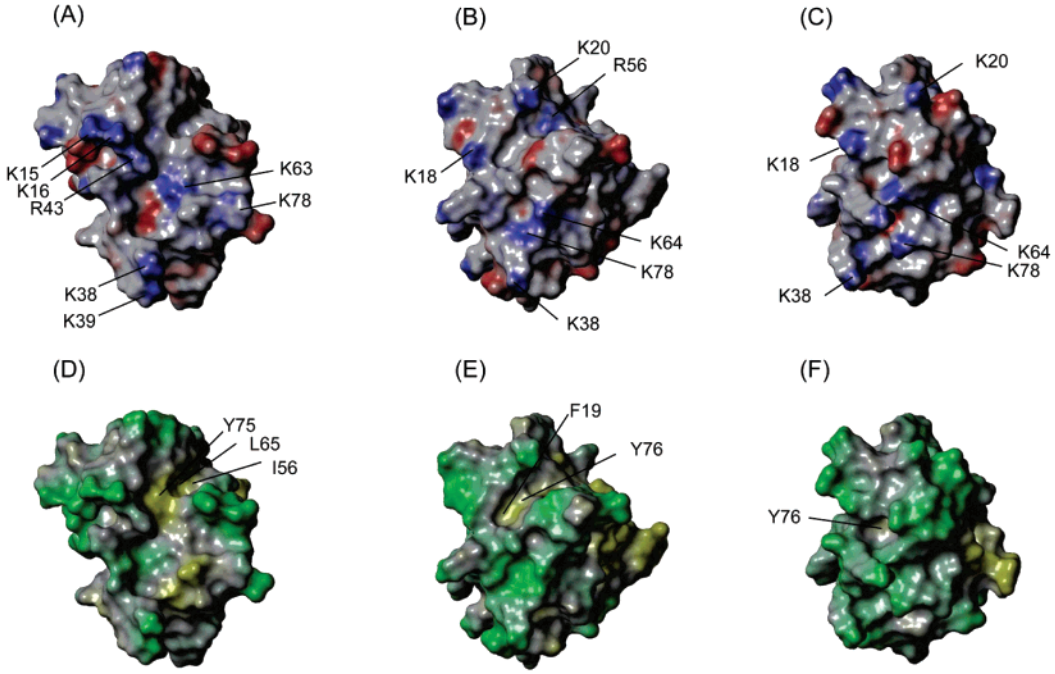

FIGURE 5: Comparison of the interaction surfaces of ADAP hSH3 domains. Panels A−C show electrostatic surface potentials of the $hSH3^C$ domain (A) and the oxidized (B) and reduced (C) $hSH3^N$ domain of ADAP. Color coding is from blue (positive potential) to red (negative potential). In panels D−F, the respective domains are shown in a representation with a color code according to a lipophilic surface potential calculated with the Sybyl software package. The color coding is yellow for lipophilic and green for hydrophilic regions of the protein surface.

displacements as large as 6.5 Å for Lys38-C_α of the RT loop. As a consequence, the two hydrogen bonds between Val37 and Phe46 cannot be formed in the oxidized $hSH3^N$, and the antiparallel orientation of the two strands of the RT loop is lost. In addition, the tip of the RT loop is placed in close proximity to the short N-terminal helix, and the side chain of Tyr76 has to flip away from the position it occupied in the reduced state, thereby making way for the side chain of Phe19 (Figure 3). Phe19, in turn, is no longer able to maintain contact to residues of the nSrc loop as it is observed in the reduced state of the domain. The liberation of the nSrc loop from the Phe19 attachment site opens a cleft between the helix-linker region and the nSrc loop. We propose that this structural epitope is likely to be occupied by an unknown binding partner in the open conformation of the oxidized $hSH3^N$ domain (see Discussion below). While the backbone rmsd for the structurally diverse elements of the two forms is 2.39 Å (colored regions in Figure 3), we find that the conserved regions of the SH3 domain scaffold superimpose more closely, with an average backbone displacement of 1.17 Å.

Lipid Binding Properties of the Reduced versus Oxidized $hSH3^N$ Domain. Despite their structural similarity with other SH3 domains (*21*), it was recently shown that hSH3 domains are lipid binding domains that have lost the ability to interact with proline-rich sequences (*20*). The structural changes we observe are in close proximity to the anticipated binding surface of the domain, and we were interested in potential differences in lipid interactions between the reduced and oxidized form of the $hSH3^N$ domain. Because PIP_2 is a likely interaction partner of ADAP in the context of T cell signaling, we determined the affinity by a vesicle cosedimentation assay. Figure 4A shows the corresponding binding curves, while Figure 4B depicts the gel analysis of a representative pull-down experiment. It can be seen that the K_D values are almost identical for the two states, when large unilamellar vesicles (LUVs) containing 54:44:2 mol % PC:PS:$PI(4,5)P_2$ are used (the K_D of reduced $hSH3^N$ is 134 ± 17 μM and the K_D of the oxidized $hSH3^N$ is 132 ± 23 μM). This indicates that binding of $hSH3^N$ to the most abundant phosphoinositide of the plasma membrane is not influenced by the redox state of the protein.

Structural Comparison of hSH3 Domains. The dissociation constants for $hSH3^N$ binding to PIP_2-containing vesicles are at least 5-fold higher than the corresponding $hSH3^C$/lipid interaction (*22*). It was argued that the higher charge of the RT loop is correlated with the higher affinity of $hSH3^C$ for acidic membranes, and this is corroborated by mutational studies showing that K39 and K63 contribute to lipid binding (*20*). Figure 5 shows a structural comparison of $hSH3^C$ (Figure 5A,D) and oxidized (Figure 5B,E) and reduced $hSH3^N$ (Figure 5C,F). Clearly, there is a contiguous and positively charged surface ridge in $hSH3^C$, including residues K15, K16, R43, K63, K38, and K39. The corresponding surface in either oxidized or reduced $hSH3^N$ is more patched and less protrusive, lending support to the hypothesis that these different surface properties modulate the charge-driven lipid interaction of hSH3 domains. Adjacent to the charged region, a lipophilic channel is formed that could accommodate several methylene groups of a lipid's hydrocarbon chain or an extended peptide structure. This region surrounding Y75 in $hSH3^C$ is well defined in the NMR structure and is not present to the same extent in $hSH3^N$ (Figure 5E,F). However, while the lipophilic channel is still partially present in oxidized $hSH3^N$ (Figure 5E), the entire site is missing in the reduced domain (Figure 5F). The existence of the channel in oxidized $hSH3^N$ is a direct consequence of the altered position of the Y76 side chain, which assumes the same relative position toward the N-terminal helix as in $hSH3^C$. Reorientation of this side chain in reduced $hSH3^N$ leads to

closing of the surface channel. This indicates that a yet to be identified lipid or protein moiety may interact with oxidized but not reduced $hSH3^N$.

DISCUSSION

Several lines of circumstantial evidence support the notion of $hSH3^N$ constituting a biologically relevant redox switch: (i) The redox potential of eukaryotic cells changes upon stimulation (*16*), and the value of −228 mV found for $hSH3^N$ is in the range that may lead to a significant fraction of oxidized ADAP in differentiating or otherwise challenged immune cells. (ii) T cells produce superoxide and hydrogen peroxide upon stimulation of the T cell receptor (*17*) and express an NADPH oxidase that is likely to locally produce ROS (*18*) and affect ADAP function. ADAP is also found at the membrane of nascent phagosomes during phagocytosis in macrophages (*38*), a process associated with oxidative burst and the production of ROS. (iii) The phosphatase SHP-2 negatively regulates ADAP phosphorylation upon T cell receptor stimulation and is part of the multiprotein complex that forms at the intracellular side of the immunological synapse (*19*). SHP-2 is inhibited by ROS upon TCR engagement, and it is likely that the ROS species are able to reach the associated ADAP molecules. Furthermore, the cysteine residues of ADAP-$hSH3^N$ are at the surface of the protein and are therefore readily accessible to ROS.

Comparison of the structures of $hSH3^C$ and $hSH3^N$ domains shows a more extended negatively charged surface of $hSH3^C$. Correspondingly, it was previously shown that $hSH3^C$ binds PC/PS/PIP_2-containing LUV's with a K_D of ∼20 μM, while $hSH3^N$ in either its oxidized or reduced form shows K_D's of ∼130 μM (Figure 4). The higher affinity of $hSH3^C$ to lipids suggests that ADAP, upon recruitment to the membrane as part of a multiprotein complex, most likely anchors its C-terminus at the lipid bilayer. Phosphorylation of the adjacent linker by membranous Fyn might then occur and initiate subsequent signaling steps. While membrane binding to $hSH3^N$ might still occur under these circumstances, the low affinity for acidic lipids suggests another bona fide binding function for the domain. However, a novel interaction partner remains elusive. It is known that ADAP tyrosine phosphorylation leads to the reversible docking of the SH2 domain containing proteins Fyn and SLP-76 (*39*, *40*), and a recent study shows that transmembrane anchoring of ADAP leads to a constitutive enhancement of adhesion, probably due to the membrane recruitment of the small GTPase Rap1 (*41*). Therefore, membrane-anchoring or posttranslational modification could be the reason that such a binding partner has not been found in yeast two-hybrid analysis or conventional pull-down experiments. More sophisticated techniques that allow the isolation of the ADAP/protein complex from cellular lysates under anaerobic conditions are needed to identify a potential redox-dependent binding partner for the domain described herein.

ACKNOWLEDGMENT

We are thankful to Katharina Thiemke for excellent technical assistance and Peter Schmieder for help with the NMR spectrometers.

REFERENCES

1. Droge, W. (2002) Free radicals in the physiological control of cell function, *Physiol. Rev. 82*, 47−95.
2. Finkel, T. (2001) Reactive oxygen species and signal transduction, *IUBMB Life 52*, 3−6.
3. Sevier, C. S., and Kaiser, C. A. (2002) Formation and transfer of disulphide bonds in living cells, *Nat. Rev. Mol. Cell Biol. 3*, 836−847.
4. Heeneman, S., Haendeler, J., Saito, Y., Ishida, M., and Berk, B. C. (2000) Angiotensin II induces transactivation of two different populations of the platelet-derived growth factor beta receptor. Key role for the p66 adaptor protein Shc, *J. Biol. Chem. 275*, 15926−15932.
5. Wang, D., Yu, X., Cohen, R. A., and Brecher, P. (2000) Distinct effects of N-acetylcysteine and nitric oxide on angiotensin II-induced epidermal growth factor receptor phosphorylation and intracellular Ca(2+) levels, *J. Biol. Chem. 275*, 12223−12230.
6. Jones, S. A., Wood, J. D., Coffey, M. J., and Jones, O. T. G. (1994) The functional expression of P47-Phox and P67-Phox may contribute to the generation of superoxide by an NADPH oxidase-like system in human fibroblasts, *FEBS Lett. 355*, 178−182.
7. Takeya, R., Ueno, N., and Sumimoto, H. (2006) Regulation of superoxide-producing NADPH oxidases in nonphagocytic cells, *Methods Enzymol. 406*, 456−468.
8. DeYulia, G. J., and Carcamo, J. M. (2005) EGF receptor-ligand interaction generates extracellular hydrogen peroxide that inhibits EGFR-associated protein tyrosine phosphatases, *Biochem. Biophys. Res. Commun. 334*, 38−42.
9. Trobaugh, D. W., Balcavage, W. X., Hughes, E. F., Waite, L. R., and Waite, G. N. (2006) Quantitative studies on biological water oxidation: a novel mechanism of T cells and antibodies, *Biomed. Sci. Instrum. 42*, 308−313.
10. Wentworth, P., Jones, L. H., Wentworth, A. D., Zhu, X. Y., Larsen, N. A., Wilson, I. A., Xu, X., Goddard, W. A., Janda, K. D., Eschenmoser, A., and Lerner, R. A. (2001) Antibody catalysis of the oxidation of water, *Science 293*, 1806−1811.
11. Abe, J., Kusuhara, M., Ulevitch, R. J., Lee, J. D., and Berk, B. C. (1996) The role of big MAP kinase 1 (BMK1) as a redox sensitive kinase in vascular smooth muscle cells, *Circulation 94*, 1627−1627.
12. Guyton, K. Z., Liu, Y. S., Gorospe, M., Xu, Q. B., and Holbrook, N. J. (1996) Activation of mitogen-activated protein kinase by H_2O_2−Role in cell survival following oxidant injury, *J. Biol. Chem. 271*, 4138−4142.
13. Hehner, S. P., Breitkreutz, R., Shubinsky, G., Unsoeld, H., Schulze-Osthoff, K., Schmitz, M. L., and Droge, W. (2000) Enhancement of T cell receptor signaling by a mild oxidative shift in the intracellular thiol pool, *J. Immunol. 165*, 4319−4328.
14. Lo, Y. Y. C., Wong, J. M. S., and Cruz, T. F. (1996) Reactive oxygen species mediate cytokine activation of c-jun NH_2-terminal kinases, *J. Biol. Chem. 271*, 15703−15707.
15. Tonks, N. K. (2005) Redox redux: revisiting PTPs and the control of cell signaling, *Cell 121*, 667−670.
16. Kirlin, W. G., Cai, J., Thompson, S. A., Diaz, D., Kavanagh, T. J., and Jones, D. P. (1999) Glutathione redox potential in response to differentiation and enzyme inducers, *Free Radical Biol. Med. 27*, 1208−1218.
17. Devadas, S., Zaritskaya, L., Rhee, S. G., Oberley, L., and Williams, M. S. (2002) Discrete generation of superoxide and hydrogen peroxide by T cell receptor stimulation: selective regulation of mitogen-activated protein kinase activation and fas ligand expression, *J. Exp. Med. 195*, 59−70.
18. Jackson, S. H., Devadas, S., Kwon, J., Pinto, L. A., and Williams, M. S. (2004) T cells express a phagocyte-type NADPH oxidase that is activated after T cell receptor stimulation, *Nat. Immunol. 5*, 818−827.
19. Kwon, J., Qu, C. K., Maeng, J. S., Falahati, R., Lee, C., and Williams, M. S. (2005) Receptor-stimulated oxidation of SHP-2 promotes T-cell adhesion through SLP-76-ADAP, *EMBO J. 24*, 2331−2341.
20. Heuer, K., Arbuzova, A., Strauss, H., Kofler, M., and Freund, C. (2005) The helically extended SH3 domain of the T cell adaptor protein ADAP is a novel lipid interaction domain, *J. Mol. Biol. 348*, 1025−1035.
21. Heuer, K., Kofler, M., Langdon, G., Thiemke, K., and Freund, C. (2004) Structure of a helically extended SH3 domain of the T cell adapter protein ADAP, *Structure (Cambridge) 12*, 603−610.
22. Heuer, K., Sylvester, M., Kliche, S., Pusch, R., Thiemke, K., Schraven, B., and Freund, C. (2006) Lipid-binding hSH3 domains in immune cell adapter proteins, *J. Mol. Biol. 361*, 94−104.
23. Geng, L., Pfister, S., Kraeft, S. K., and Rudd, C. E. (2001) Adaptor FYB (Fyn-binding protein) regulates integrin-mediated adhesion

and mediator release: differential involvement of the FYB SH3 domain, *Proc. Natl. Acad. Sci. U.S.A 98*, 11527−11532.
24. Griffiths, E. K., Krawczyk, C., Kong, Y. Y., Raab, M., Hyduk, S. J., Bouchard, D., Chan, V. S., Kozieradzki, I., Oliveira-Dos-Santos, A. J., Wakeham, A., Ohashi, P. S., Cybulsky, M. I., Rudd, C. E., and Penninger, J. M. (2001) Positive regulation of T cell activation and integrin adhesion by the adapter Fyb/Slap, *Science 293*, 2260−2263.
25. Peterson, E. J., Woods, M. L., Dmowski, S. A., Derimanov, G., Jordan, M. S., Wu, J. N., Myung, P. S., Liu, Q. H., Pribila, J. T., Freedman, B. D., Shimizu, Y., and Koretzky, G. A. (2001) Coupling of the TCR to integrin activation by Slap-130/Fyb, *Science 293*, 2263−2265.
26. Kraulis, P. J. (1989) Ansig−A program for the assignment of protein H-1 2D-NMR spectra by interactive computer-graphics, *J. Magn. Reson. 84*, 627−633.
27. Kraulis, P. J., Domaille, P. J., Campbellburk, S. L., Vanaken, T., and Laue, E. D. (1994) Solution structure and dynamics of Ras P21·GDP determined by heteronuclear 3-dimensional and 4-dimensional NMR-spectroscopy, *Biochemistry 33*, 3515−3531.
28. Guntert, P., Mumenthaler, C., and Wuthrich, K. (1997) Torsion angle dynamics for NMR structure calculation with the new program DYANA, *J. Mol. Biol. 273*, 283−298.
29. Guntert, P. (2004) Automated NMR structure calculation with CYANA, *Methods Mol. Biol. 278*, 353−378.
30. Herrmann, T., Guntert, P., and Wuthrich, K. (2002) Protein NMR structure determination with automated NOE assignment using the new software CANDID and the torsion angle dynamics algorithm DYANA, *J. Mol. Biol. 319*, 209−227.
31. Zimmermann, J., and Freund, C. (2005) NMR assignment of the reduced and oxidized forms of the human ADAP hSH3-1 domain, *J. Biomol. NMR 32*, 94.
32. Cornilescu, G., Delaglio, F., and Bax, A. (1999) Protein backbone angle restraints from searching a database for chemical shift and sequence homology, *J. Biomol. NMR 13*, 289−302.
33. Nabuurs, S. B., Nederveen, A. J., Vranken, W., Doreleijers, J. F., Bonvin, A. M. J. J., Vuister, G. W., Vriend, G., and Spronk, C. A. E. M. (2004) DRESS: a database of refined solution NMR structures, *Proteins: Struct., Funct., Bioinf. 55*, 483−486.
34. Koradi, R., Billeter, M., and Wuthrich, K. (1996) MOLMOL: a program for display and analysis of macromolecular structures, *J. Mol. Graphics 14*, 51−55.
35. Laskowski, R. A., Rullmannn, J. A., MacArthur, M. W., Kaptein, R., and Thornton, J. M. (1996) AQUA and PROCHECK-NMR: programs for checking the quality of protein structures solved by NMR, *J. Biomol. NMR 8*, 477−486.
36. Gryk, M. R., Abseher, R., Simon, B., Nilges, M., and Oschkinat, H. (1998) Heteronuclear relaxation study of the PH domain of beta-spectrin: restriction of loop motions upon binding inositol trisphosphate, *J. Mol. Biol. 280*, 879−896.
37. Schafer, F. Q., and Buettner, G. R. (2001) Redox environment of the cell as viewed through the redox state of the glutathione disulfide/glutathione couple, *Free Radical Biol. Med. 30*, 1191−1212.
38. Coppolino, M. G., Krause, M., Hagendorff, P., Monner, D. A., Trimble, W., Grinstein, S., Wehland, J., and Sechi, A. S. (2001) Evidence for a molecular complex consisting of Fyb/SLAP, SLP-76, Nck, VASP and WASP that links the actin cytoskeleton to Fcgamma receptor signalling during phagocytosis, *J. Cell Sci. 114*, 4307−4318.
39. da Silva, A. J., Li, Z., de Vera, C., Canto, E., Findell, P., and Rudd, C. E. (1997) Cloning of a novel T-cell protein FYB that binds FYN and SH2-domain-containing leukocyte protein 76 and modulates interleukin 2 production, *Proc. Natl. Acad. Sci. U.S.A 94*, 7493−7498.
40. Musci, M. A., Hendricks-Taylor, L. R., Motto, D. G., Paskind, M., Kamens, J., Turck, C. W., and Koretzky, G. A. (1997) Molecular cloning of SLAP-130, an SLP-76-associated substrate of the T cell antigen receptor-stimulated protein tyrosine kinases, *J. Biol. Chem. 272*, 11674−11677.
41. Kliche, S., Breitling, D., Togni, M., Pusch, R., Heuer, K., Wang, X., Freund, C., Kasirer-Friede, A., Menasche, G., Koretzky, G. A., and Schraven, B. (2006) The ADAP/SKAP55 signaling module regulates T-cell receptor-mediated integrin activation through plasma membrane targeting of Rap1, *Mol. Cell. Biol. 26*, 7130−7144.

BI700437R